ARTICLES

Measurements of $^1H(\vec{d},\gamma)^3He$ and $^2H(\vec{p},\gamma)^3He$ at very low energies

L. Ma, H. J. Karwowski, C. R. Brune, Z. Ayer, T. C. Black, J. C. Blackmon, and E. J. Ludwig
Department of Physics and Astronomy, University of North Carolina at Chapel Hill, Chapel Hill, North Carolina 27599-3255 and Triangle Universities Nuclear Laboratory, Durham, North Carolina 27708

M. Viviani and A. Kievsky
Istituto Nazionale di Fisica Nucleare, Piazza Torricelli 2, 56100 Pisa, Italy

R. Schiavilla
Jefferson Lab Theory Group, Newport News, Virginia 23606 and Department of Physics, Old Dominion University, Norfolk, Virginia 23529

(Received 30 August 1996)

Angular distributions of the analyzing powers iT_{11}, T_{20}, and T_{22} for $^1H(\vec{d},\gamma)^3He$ at $40 \leqslant E_{c.m.} \leqslant 110$ keV and the angular distribution of the analyzing power A_y for $^2H(\vec{p},\gamma)^3He$ at $70 \leqslant E_{c.m.} \leqslant 210$ keV have been measured for the first time. In addition, absolute differential cross sections for proton-deuteron capture have been determined for $E_{c.m.} = 75$, 108, 133, and 173 keV. Thick ice or heavy ice targets and two large-volume, high-purity Ge γ-ray detectors were used. Results are in general agreement with an exact three-body calculation utilizing a realistic nucleon-nucleon potential. The vector-polarization observables are found to be especially sensitive to meson-exchange-current effects. The extracted $S(0)$ value for proton-deuteron capture is $\sim 25\%$ lower than that presently used in astrophysical calculations. An expression for the thermonuclear reaction rate below 10 GK is given. [S0556-2813(97)04502-0]

PACS number(s): 21.45.+v, 24.70.+s, 25.10.+s, 25.40.Lw

I. INTRODUCTION

The proton-deuteron capture reaction at low energies is very useful for studying the bound ^{3}He system [1,2] and the reaction mechanism of radiative capture, particularly the role of meson exchange currents (MEC's) [3]. The cross section for proton-deuteron capture is an important parameter in models of big-bang nucleosynthesis [4], stellar hydrogen burning [5], and deuterium depletion in low-mass protostars, which is believed to be essential for their genesis and evolution [6]. The big-bang production of deuterium is currently of great interest, due to recent measurements of the D/H ratio in high-redshift hydrogen clouds [7]. The D/H ratio in these clouds is thought to reflect the primordial abundance, and may soon place tight constraints on big-bang nucleosynthesis models.

In this paper we report the measurements of polarization observables and differential cross sections for proton-deuteron capture. The primary goal of these measurements is to test exact three-body calculations of this reaction, which include MEC effects. Reported here are calculations using three-body wave functions obtained with a recently developed variational method which provides the wave functions in a pair-correlated–hyperspherical-harmonics (PHH) function basis. The method makes use of realistic nucleon-nucleon (NN) and three-body forces, and utilizes an electromagnetic current operator which includes one- and two-body terms. The PHH model has already been successfully applied in several areas of few-body nuclear physics [8,9].

In addition, a recent measurement of the $^2H(p,\gamma)^3He$ cross section for $E_{c.m.} < 50$ keV by another group [10,11] indicates a significantly lower $S(0)$ value compared with previous determinations [12–14]. The new absolute cross section data reported here aid in resolving this discrepancy. The thermonuclear reaction rate is calculated as a function of temperature from all available data, and the effect of this new reaction rate on standard big-bang nucleosynthesis is assessed. A detailed description of the experimental technique and data analysis are available in Ref. [15].

II. EXPERIMENTAL PROCEDURE

The measurements of iT_{11}, T_{20}, and T_{22} for $^1H(\vec{d},\gamma)^3He$ and A_y and the differential cross section for $^2H(\vec{p},\gamma)^3He$ were carried out using the low-energy beam facility at the Triangle Universities Nuclear Laboratory, as described below.

A. Beam

Up to 10 μA of negative polarized proton or deuteron beam was produced using an atomic-beam polarized ion source [16]. The beam was accelerated using the minitandem accelerator [17], yielding 2–4 μA of polarized particles on target with an energy of up to 350 keV. The energy calibration of the minitandem beam was determined to $\pm 1\%$ using the 224.0- and 340.5-keV resonances in $^{19}F(p,\alpha\gamma)^{16}O$.

The analyzing powers were measured using a fast spin-flip scheme. The desired hyperfine states of atomic hydrogen or deuterium were cycled approximately every second. This technique minimizes the effects of slow changes in beam position, target thickness, or amplifier gain.

For the proton beam measurements, the Wien filter was set to align the spin axis perpendicular to the reaction plane ($\beta=90°$). Proton polarization was determined by accelerating the beam with the FN tandem to $E_p=6$ MeV. Elastically scattered protons from $^4He(\vec{p},p)$ were detected using symmetrically placed left and right detectors at $\theta_{lab}=117°$, where the analyzing power is nearly unity [18,19]. The proton data were taken using two spin states with $p_y\approx\pm0.7$. The systematic uncertainty in the proton polarization is estimated to be $<4\%$, which could affect the overall normalization of the measured analyzing powers. Since the systematic uncertainty is estimated to be significantly less than the statistical uncertainties for all measured observables, they are not included in the data presented here.

The polarization of the deuteron beam was determined with the $^3He(\vec{d},p)^4He$ reaction at $E_d=12$ MeV using the FN tandem [20] and also at $E_d=0.33$ MeV using the minitandem [21]. The polarized deuteron data were taken using two hyperfine transitions with a theoretical maximum tensor polarization of $p_{zz}=\pm1$ and a maximum vector polarization of $p_z=\mp1/3$. Typical measured values were $p_{zz}\approx\pm0.7$ and $p_z\approx\mp0.2$. The T_{20} data were taken with the spin axis set parallel to the incident beam axis ($\beta=0°$). The analyzing powers A_{yy} and iT_{11} were measured with the spin perpendicular to the reaction plane ($\beta=90°$). The analyzing power T_{22} was then determined from the measured A_{yy} and T_{20} values. The systematic uncertainty in the tensor polarizations is estimated to be $<4\%$, while the systematic uncertainty in the deuteron vector polarization is estimated to be $<6\%$.

The proton or deuteron polarizations were measured on a regular basis (4–6 h period) and were found to be stable within less than 2%.

B. Targets

The target consisted of a thick layer of vapor-condensed ice or heavy ice of sufficient thickness to completely stop the incident beam. The construction of the target condensing assembly [15] was based on the design used by Griffiths *et al.* [13]. High-purity deuterated water (D_2O) was used for the $^2H(\vec{p},\gamma)^3He$ measurements. For the $^1H(\vec{d},\gamma)^3He$ measurements, deuterium-depleted H_2O (<1 ppm D_2O) was used in order to minimize the neutron-induced background from the $^2H(d,n)$ reaction. The targets were periodically melted and then remade, in order to minimize the neutron-induced background. The target assembly was electrically isolated and biased with $+90$ V to insure correct beam current integration.

C. γ-ray detection

The energy of the capture γ rays is given approximately by $E_\gamma=Q+E_{c.m.}$, where $Q=5.494$ MeV is the Q value for proton-deuteron capture, and $E_{c.m.}$ is the reaction energy in the center-of-mass frame. Since a thick target is used, $E_{c.m.}$ varies between 0 and incident center-of-mass energy of the incident beam, giving rise to broadened γ-ray peak. The resulting γ rays were detected by two high-purity germanium (HPGe) detectors. The efficiencies of the two detectors for 1.33-MeV γ rays are 128 and 145 %, relative to a 7.62-cm-diam $\times$ 7.62-cm-length NaI scintillator. The resolution of the detectors was typically 2.0 keV at 1.33-MeV γ ray from the decay of ^{60}Co. The use of high-resolution γ-ray detectors and targets sufficiently thick to stop the beam allowed the energy dependence of the observables to be extracted at each detection angle.

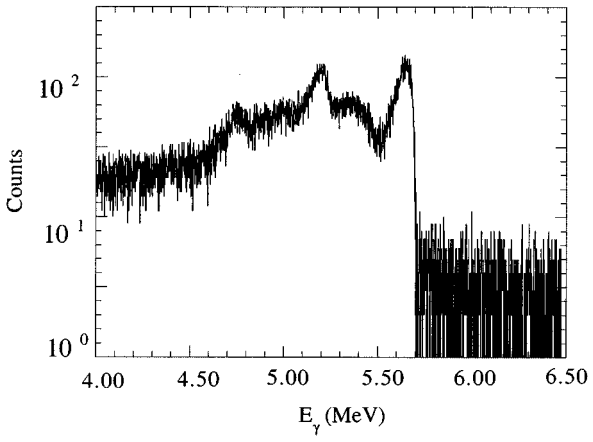

FIG. 1. A typical γ-ray spectrum from the $^2H(\vec{p},\gamma)^3He$ reaction, measured at $\theta_{lab}=60°$ with 312-keV protons incident on the target.

Typical γ-ray spectra from the $^2H(\vec{p},\gamma)^3He$ and $^1H(\vec{d},\gamma)^3He$ reactions are shown in Figs. 1 and 2. The γ-ray spectrum shown in Fig. 1 resulted from reactions induced by 312-keV protons incident on heavy ice, with the 128% HPGe detector at $\theta_{lab}=60°$. The background adjacent to the high-energy edge of the full-energy peak is approximately 50 times smaller than the height of the full-energy peak, and has a smooth energy dependence. The γ-ray spectrum from $^1H(\vec{d},\gamma)^3He$ shown in Fig. 2 was obtained by

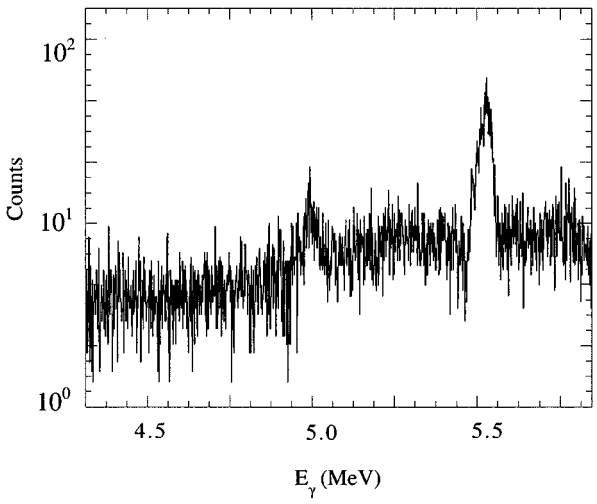

FIG. 2. A typical γ-ray spectrum from the $^1H(\vec{d},\gamma)^3He$ reaction, measured at $\theta_{lab}=90°$ with 330-keV protons incident on the target.

bombarding an ice target with 330-keV deuterons, and observing photons with the 145% HPGe detector at $\theta_{lab}=90°$. The background in this spectrum is considerably higher than observed in the case of the $^2H(\vec{p},\gamma)^3He$ reaction. This background is mainly due to neutron-induced reactions, with $^2H(d,n)^3He$ being the primary source of neutrons. Despite the use of deuterium-depleted H_2O, a significant quantity of deuterium was built up in the target over time due to implantation by the beam, thus providing target nuclei for the $^2H(d,n)^3He$ reaction. Tests with a neutron source revealed that no neutron-induced peaks were within the region of interest, so the background was modeled by a smooth function of γ-ray energy.

D. Detector efficiency

The full-energy-peak absolute efficiencies (FAE's) used in the cross section measurements were determined experimentally. The efficiencies reported here have been normalized by the solid angle subtended by the front face of the Ge crystal. At γ-ray energies of 1.33, 1.77, and 1.86 MeV, the absolute efficiencies were measured using a calibrated radioactive source commercially available from Amersham Corporation (source code QCD.1). The absolute efficiency at a γ-ray energy of 6.13 MeV was determined using the 340-keV resonance in the $^{19}F(p,\alpha\gamma)^{16}O$ reaction [12]. The measurement was carried out using a 346-keV proton beam incident on a ≈ 50-$\mu g/cm^2$-thick CaF_2 target. The resulting α particles and 6.13-MeV γ rays are emitted in one-to-one coincidence, and to a good approximation they are emitted isotropically in the center-of-mass system. This technique is superior to the ^{66}Ga source calibration used previously since it avoids using poorly known branching ratios and extrapolations. More information on the $^{19}F(p,\alpha\gamma)^{16}O$ efficiency calibration techinque is available in Ref. [22].

The α particles and γ rays were detected simultaneously. Assuming that the intrinsic efficiency of α-particle detection by a surface-barrier solid state detector is 100%, the FAE for the HPGe detector was determined by the counting ratios of detected γ rays and the α particles. Since the solid angle subtended by the Si detector is known, the absolute efficiency of the HPGe could be easily determined. The FAE for the HPGe detector for the cross section measurements was thus determined to be 0.0894 ± 0.0010, where the error indicates the statistical uncertainty only. The systematic uncertainty is estimated to be $<4\%$.

The measured absolute efficiencies at all energies were fitted with a function in the form of $P_1E_\gamma^{P_2}$, where E_γ is the γ-ray energy in MeV and P_1 and P_2 are the fit parameters. Their resulting values are $P_1=0.2530\pm0.0019$ and $P_2=-0.5739\pm0.0083$. The efficiency data together with the fitted curve are shown in Fig. 3. The interpolated absolute efficiency at $E_\gamma=5.7$ MeV is 0.0932 ± 0.0011, and this value is used for the cross section determinations.

In addition the absolute efficiency for the full-energy γ-ray peak was calculated using Monte Carlo simulations with the GEANT 3.15 code [23]. These calculations yield an efficiency of 0.0964 for $E_\gamma=5.7$ MeV, which agrees within 4% with the experimental value.

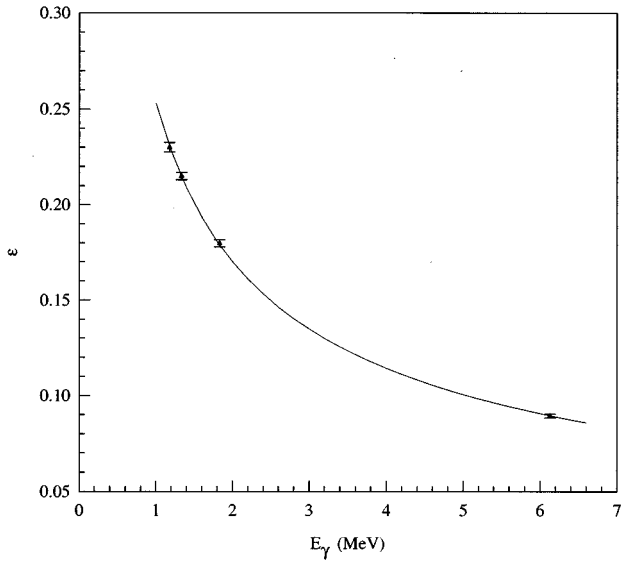

FIG. 3. Absolute full-energy peak efficiencies for the 128% HPGe detector used for the absolute cross section measurements. The results have been normalized by the solid angle subtended by the front face of the HPGe crystal. The solid line is the best fit to the data, described in the text.

III. DATA ANALYSIS

A. Cross section data

The cross section was determined from the $^2H(\vec{p},\gamma)^3He$ data by dividing the full-energy peak of the spectrum into several bins in γ-ray energy. Four energy bins centered at center-of-mass energies of 75, 108, 133, and 173 keV were chosen, insuring the statistical significance of the total number of counts inside each energy bin. The total number of counts in each bin was used to determine the yield for the γ-ray energy averaged over the width of the bin. The data for the two proton spin states were combined, which amounts to essentially unpolarized beam, since the polarizations of the two states are nearly opposite (the error introduced by this procedure is negligible).

B. Analyzing power data

The analyzing powers are normally calculated from the ratio of two yields resulting from reactions initiated by beams prepared in two different spin populations. As has been discussed previously, the measured full-energy peak represents a total yield integrated over a γ-ray energy ranging from $E_\gamma=E_{c.m.}+Q$ down to $E_\gamma=Q$. Therefore, the ratio of the integrated yields measured for different spin states is not directly related to the analyzing powers at a single γ-ray energy. Moreover, such a ratio cannot be used for determining analyzing powers for an ''average'' energy, since any algebra on the analyzing powers, e.g., averaging over an energy range, is always performed on the ratio of the yields at a single energy rather than on its numerator or denominator separately.

We have therefore developed a functional deconvolution method in order to determine the analyzing powers from the full-energy peak. The shape of the full-energy peak was fitted using the following formula:

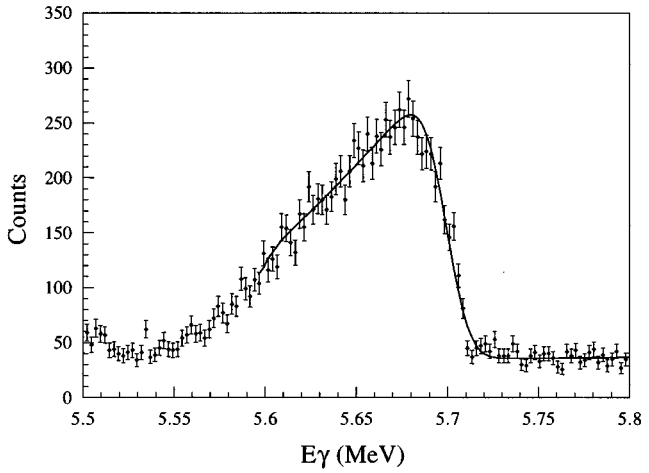

FIG. 4. A typical convolution fit to the full-energy peak for one spin state of the beam.

$$Y(E_\gamma)=\int_{E_i}^{E_f} d\xi R(E_\gamma-\xi)T(\xi)\frac{\exp(-2\pi\eta)}{\xi}G(\xi), \quad (1)$$

where E_γ is the γ-ray energy, ξ is the center-of-mass energy, $Y(E_\gamma)$ is the energy dependence of total yield, R is the detector response function, T describes the beam stopping effects, $\eta=e^2Z_1Z_2/\hbar v$ is the Sommerfeld parameter, and G describes the remaining energy dependence of the polarized cross section.

The detector response function $R(E_\gamma-\xi)$ is taken to be of the empirical form given by Jorsch and Campbell [24]. Its functional form is composed of a Gaussian with a small low-energy tail. The function $T(\xi)$ is given by the inverse of the energy dependence for the stopping power of hydrogen or deuterium ions in the ice target. The stopping powers were calculated using the TRIM92 code of Ziegler [25]. For the case of protons stopping in an ice target, the calculation agrees with the experimental data [26] within 5%. Since the astrophysical S factor for the proton-deuteron capture is expected to be a smooth and slowly varying function of energy, the quantity $G(\xi)$ was expanded into a polynomial series as follows:

$$G(\xi)=\sum_{i=0}^{n} P_i\xi^i, \quad (2)$$

where the P_i's are the fitting coefficients, and n is usually truncated to 2. This polynomial expansion in reaction energy is found for each spin state, and is used to represent the spin-dependent yields needed to calculate the analyzing powers.

In order to obtain all the fitting coefficients P_i, the MINUIT fitting routine [27] was programmed and applied to fit the full-energy peak with the functional form of $Y(E_\gamma)$ for each spectrum corresponding to each spin-population state of the beam. A typical fitted $^1H(p,\gamma)^3He$ spectrum is shown in Fig. 4. The error matrices for the fitting parameters were also calculated using MINUIT and were later used for error propagation when evaluating the energy-dependent analyzing powers.

IV. RESULTS

A. Analyzing powers

The energy dependence of iT_{11}, T_{20}, and T_{22} for $^1H(d,\gamma)^3He$ have been obtained at $40\leqslant E_{\text{c.m.}}\leqslant 110$ keV for six center-of-mass angles: 0° (for T_{20} only), 38°, 61°, 91°, 121°, and 137°. The energy dependence of A_y for $^2H(\vec{p},\gamma)^3He$ has been obtained for $70\leqslant E_{\text{c.m.}}\leqslant 212$ keV at three center-of-mass angles: 31°, 61°, and 91°. In Fig. 5, the energy dependences of all measured analyzing powers are presented for $\theta_{\text{c.m.}}=91°$. The $^2H(\vec{p},\gamma)^3He$ data were taken with two incident energies, $E_p=242$ and 312 keV. These data were analyzed separately, leading to the discontinuity in

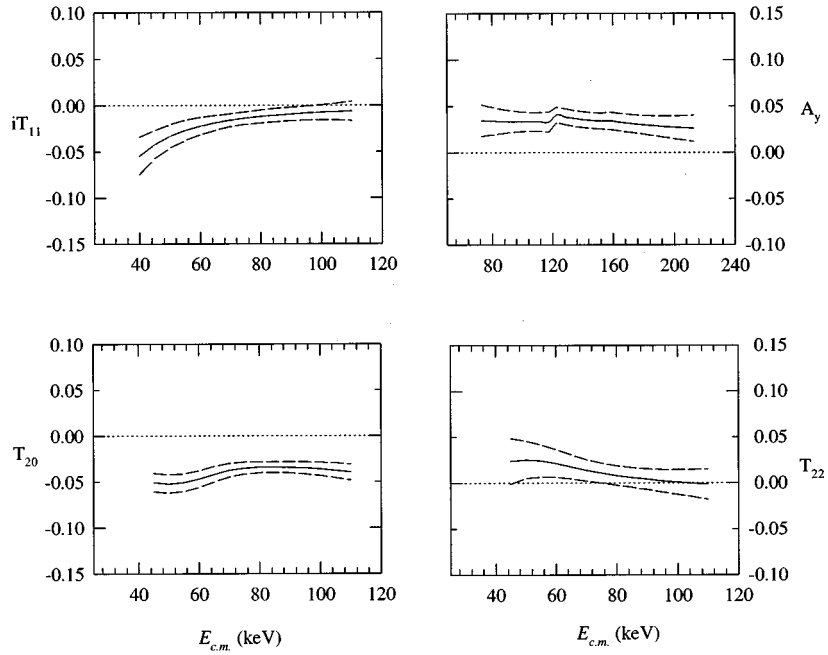

FIG. 5. Energy dependence of the measured analyzing powers at $\theta_{\text{c.m.}}=91°$.

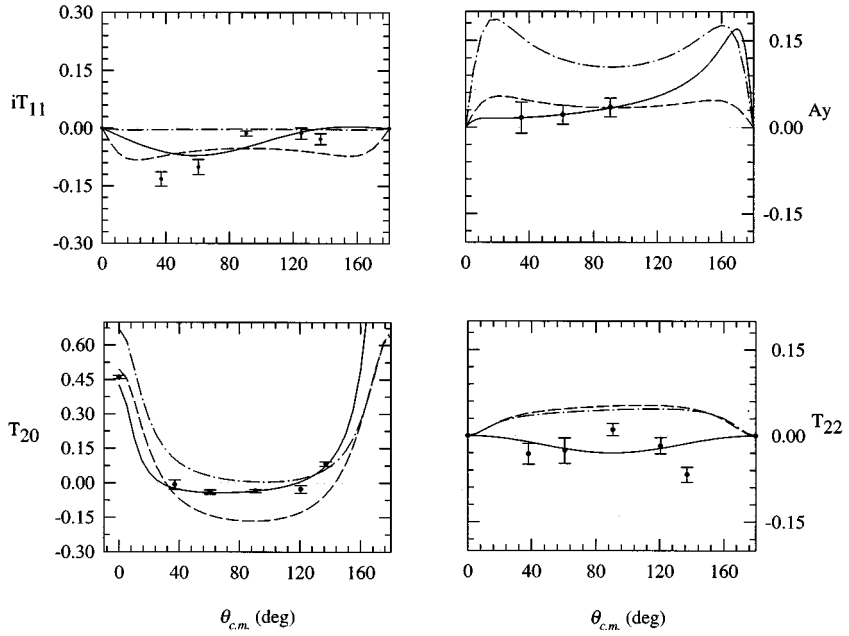

FIG. 6. Angular distributions of the measured analyzing powers at $E_{\text{c.m.}}=75$ keV. The solid lines are the best Legendre fits, the dashed lines are the full PHH model calculations, and the dot-dashed lines are the impulse-approximation results.

the A_y data in Fig. 5. The $^1\text{H}(\vec{d},\gamma)^3\text{He}$ data were taken with an incident energy of $E_d=330$ keV. The dashed-line-enclosed region represents an error band of 1-σ confidence level. The angular distribution data at $E_{\text{c.m.}}=75$ and 100 keV are shown in Figs. 6 and 7.[1] The significance curves in Figs. 6 and 7 is described below in Secs. IV B and V C.

The present analyzing power results are the first ever obtained in this energy range. There has been only one other low-energy measurement of A_y for $^2\text{H}(\vec{p},\gamma)^3\text{He}$ at $E_{\text{c.m.}}<50$ keV [10,11]; all other previous measurements were performed at $E_{\text{c.m.}}>500$ keV.

B. Legendre polynomial fits

Legendre polynomial fits to the data were carried out following the prescription given in Refs. [28,29]. The differential cross section data were fitted using only $l=0$ and $l=2$ terms in the expansion (l is the order of the polynomial), as previous measurements in this energy range found other terms to be negligible [12,14]. For the analyzing power fits, the expansions were truncated after $l=2$, as previous analyses at higher energies [29,30] found these terms to be very small. Furthermore, coefficients with $l\geqslant 3$ requires the presence of $E2$ capture amplitudes, which are expected to be very small at low energies due to γ-ray phase space considerations. The fits are shown by the solid lines in Figs. 6 and 7. The coefficients for $E_{\text{c.m.}}=75$ keV are given in Table I.

C. Total cross sections

The total cross section was determined at four energies: $E_{\text{c.m.}}=75$, 108, 133, and 173 keV, using the fits to the differential cross section described in the previous subsection. The results are shown in Fig. 8 along with the previous measurements within the same energy range [12,14]. The systematic uncertainty for the cross sections is estimated to be $\pm 9\%$, and includes the estimated errors in stopping power, detector efficiency, γ-ray angular distribution assumptions, and beam current integration.

The astrophysical S factors $[S(E)=\sigma_{\text{tot}}Ee^{2\pi\eta}]$ are shown in Fig. 9 along with previous measurements.

V. THEORETICAL CALCULATIONS

The transition amplitude between an initial $d+p$ continuum state with deuteron and proton spin projections σ_2 and σ, respectively, and relative momentum $\mathbf{p}$, and a final ^{3}He state with spin projection σ_3 is given by

$$j^{\alpha}_{\sigma_3\sigma_2\sigma}(\mathbf{p},\mathbf{q})=\left\langle \psi_{\sigma_3}\middle|\boldsymbol{\epsilon}_{\alpha}\cdot\int d\mathbf{x}\,e^{-i\mathbf{q}\cdot\mathbf{x}}\mathbf{j}(\mathbf{x})\middle|\psi^{(+)}_{\mathbf{p},\sigma_2\sigma}\right\rangle, \quad (3)$$

where $\boldsymbol{\epsilon}_{\alpha}$ is the polarization of the photon, $\mathbf{j}(\mathbf{x})$ is the nuclear current density, and $\psi^{(+)}$ is the scattering wave function with outgoing wave boundary condition. Expressions for the cross section, vector, and tensor analyzing powers, and photon linear polarization are easily obtained from the amplitudes $j^{\alpha}_{\sigma_3\sigma_2\sigma}$ [1]. A schematic description of the trinucleon wave functions and the current density is included below. A thorough discussion of the various issues relating to them, however, can be found in Ref. [1].

A. The trinucleon wave functions

In a series of recent papers, a variational technique for calculating the ^{3}H and ^{3}He bound states and the $d+N$ elastic scattering state wave functions has been developed [8,9,31]. For bound states, the method utilizes an expansion of the three-body wave functions in terms of a pair-correlated hyperspherical harmonic (PHH) function basis. The Rayleigh-Ritz variational principle is used to determine the hyperradial functions which determine the wave func-

[1]All numerical data tables for the energy or angular dependences are available from the authors upon request.

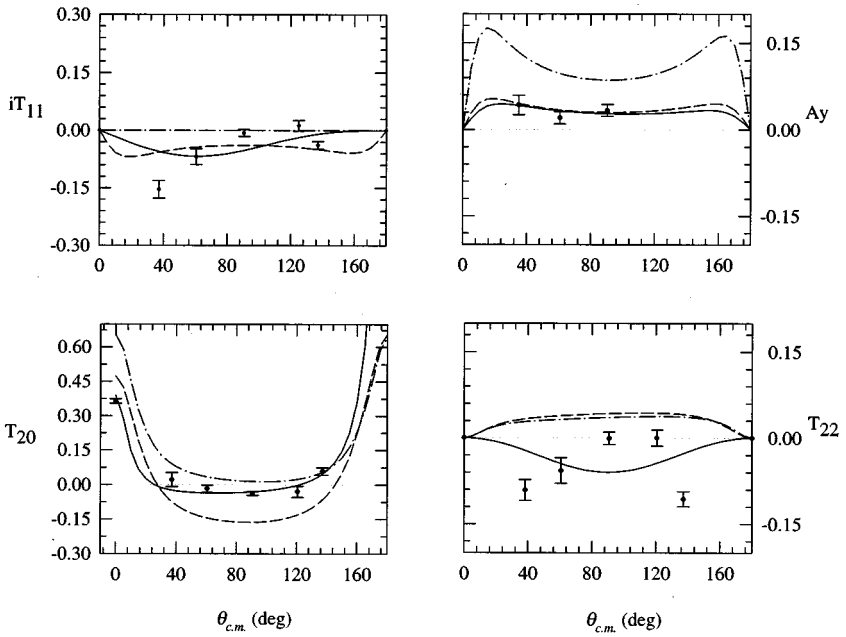

FIG. 7. Angular distribution of the measured analyzing powers at $E_{\text{c.m.}}=100$ keV. The lines have the same meaning as in Fig. 6.

tion. The resulting coupled set of second-order differential equations is solved by using standard numerical methods. The inclusion of the Coulomb interaction is straightforward, as no partial wave decomposition is performed.

The variational approach based on PHH correlated functions has been extended to investigate scattering states. The wave function for a $d+p$ scattering state is written as

$$\Psi^{JJ_zLS}_{2+1}=\Psi^{JJ_zLS}_{C}+\Psi^{JJ_zLS}_{A}, \tag{4}$$

where J and J_z are the total angular momentum and its z projection, L is the $d+p$ relative orbital angular momentum and S the channel spin quantum number, respectively. The first term Ψ_C describes the ''core'' of the system, when all the particles are close to each other and the mutual interactions are large; Ψ_C goes to zero when the proton-deuteron distance r_{pd} increases. Ψ_C is expanded in terms of the PHH basis functions, as in the bound-state case. The second term Ψ_A in Eq. (4) describes the asymptotic configurations of the system, for large r_{pd} where the nuclear $d+p$ interactions are negligible. In the asymptotic region the wave function Ψ_{2+1} reduces to Ψ_A, which must therefore be the appropriate asymptotic solution of the Schrödinger equation.

The reaction-matrix elements $^JR^{L'S'}_{LS}$ and the hyperradial functions entering in the PHH expansion of Ψ_C are determined variationally by finding the stationary points of the functional [9]

TABLE I. The best-fit Legendre coefficients for the measured observables at $E_{\text{c.m.}}=75$ keV. The uncertainties in the least significant digits are given in parentheses. The definition of the coefficients follows Seyler and Weller [28].

l	σ	A_y	iT_{11}	T_{20}	T_{22}
0	1.00	-	-	−0.011(5)	-
1	0.00	−0.05(2)	0.09(1)	−0.052(6)	-
2	−0.96	0.01(1)	0.03(1)	0.070(4)	−0.06(1)

$$[{}^JR^{LS}_{LS}]={}^JR^{LS}_{LS}-\left\langle \psi^{JJ_zLS}_{2+1}\middle| H-E_d-\frac{3}{4m}p^2\middle|\psi^{JJ_zLS}_{2+1}\right\rangle, \tag{5}$$

with respect to variations in the $^JR^{L'S'}_{LS}$ and the hyperradial functions (Kohn variational principle). Here $E_d=-2.225$ MeV is the deuteron binding energy. As in the bound state problem, the hyperradial functions are required to vanish in the limit of large ρ.

The Hamiltonian used in the present calculations consists of the Argonne v_{18} two-nucleon [32] and Urbana model-IX three-nucleon [33] interactions. The ^{3}He binding energy obtained with the PHH wave functions reproduces the measured value. It is worth emphasizing that predictions based on PHH wave functions for a variety of other properties, depending on both ground and low-energy continuum states

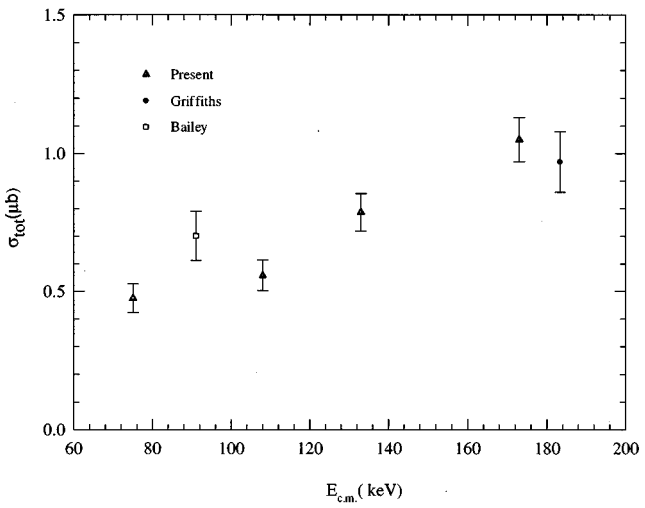

FIG. 8. Measured total cross sections for proton-deuteron capture, compared to the previous measurements in our energy range by Bailey *et al.* [14] and Griffiths, Larson, and Robertson [12].

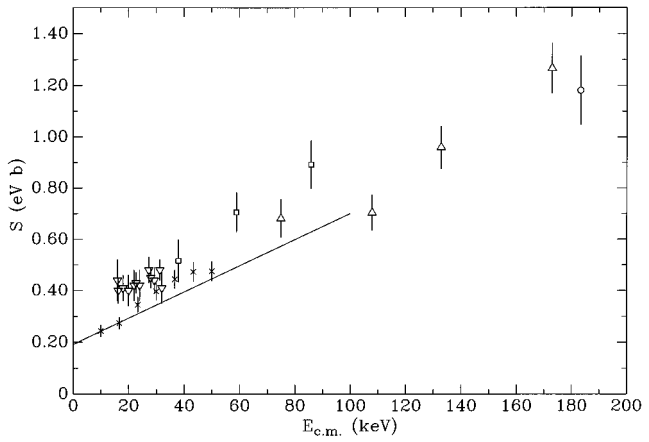

FIG. 9. Measured S factors ($\triangle$) compared with the previous measurements Schmid *et al.* [11] ($\times$), Bailey *et al.* [14] ($\square$), Griffiths, Lal, and Scarfe [13] ($\triangledown$), and Griffiths, Larson, and Robertson [12] ($\bigcirc$). The PHH model calculations are shown by the solid curve.

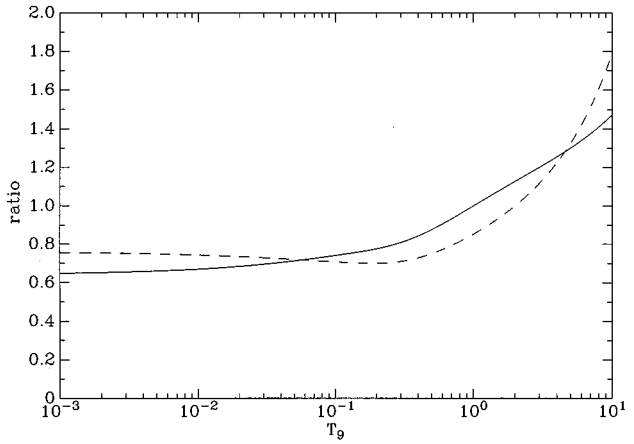

FIG. 10. The ratio of the present reaction rate [Eq. (9)] to that given by Smith, Kawano, and Malaney [4] (solid line) and to that given by Caughlin and Fowler [38] (dashed line).

of the trinucleon, are in excellent agreement with corresponding Faddeev calculations [31].

B. The transition current

The nuclear current density is represented by effective operators that operate on the nucleons' degrees of freedom. These operators are expanded into sums of one-, two-, and many-body terms:

$$\mathbf{j}(\mathbf{q})=\sum_i \mathbf{j}_i^{(1)}(\mathbf{q})+\sum_{i<j}\mathbf{j}_{ij}^{(2)}(\mathbf{q})+\cdots. \tag{6}$$

The one-body terms $\mathbf{j}^{(1)}(\mathbf{q})$ have the standard impulse approximation form, consisting of the single-nucleon convection and spin-magnetization currents, while the two-body terms $\mathbf{j}^{(2)}(\mathbf{q})$ consist of ''model-independent'' and ''model-dependent'' parts [34–36] [the expansion of Eq. (6) is truncated at the two-body level in the results discussed here].

The ''model-independent'' $\mathbf{j}^{(2)}(\mathbf{q})$ terms do not contain any free parameters, and are constructed from the pair interaction v_{ij} (here, the Argonne v_{18} [32]), following a prescription originally proposed by Riska [37]. These terms are necessary to satisfy the continuity equation.

The ''model-dependent'' $\mathbf{j}^{(2)}(\mathbf{q})$ terms, such as those associated with the $\rho\pi\gamma$ and $\omega\pi\gamma$ processes, are purely transverse and therefore unconstrained by v_{ij}. Furthermore, they depend on a set of cutoff parameters and coupling constants only approximately known. Their contribution for momentum transfers $\leqslant 1$ GeV/c is small when compared to that of the leading ''model-independent'' two-body currents.

The currents associated with the excitation of the Δ resonance are included nonperturbatively following a method first proposed in Ref. [34]. In essence, the Δ degrees of freedom are explicitly included in the nuclear wave functions rather than being eliminated in favor of effective two-body operators acting on the nucleons' coordinates. The latter perturbative treatment has been shown to be inaccurate, particularly in reactions as delicate as the $^3\mathrm{He}(n,\gamma)^4\mathrm{He}$ and $^3\mathrm{He}(p,e^+\nu_e)^4\mathrm{He}$ captures at low energies [34]. For the present reaction, however, it only leads to an $\simeq$ 8% overestimate of the doublet $M1$ reduced matrix element when compared to the result obtained with the more accurate nonperturbative treatment [1].

Finally, we note that the continuity equation also requires the presence of three-body currents associated with the three-nucleon interactions. To the best of our knowledge, their effect has not yet been studied.

C. Theoretical results

In Figs. 6 and 7 the comparison of the PHH calculations with the polarization data is shown for $E_{\mathrm{c.m.}}=75$ and 100 keV. Two different models were used for this comparison. The dot-dashed lines show the calculations performed using only the impulse approximation matrix elements (i.e., without MEC). The dashed lines represent the full calculation including MEC. The marked improvement in the agreement with the data shows that the inclusion of MEC is very important for describing the angular dependence of the analyzing powers. In particular, the A_y curve for the full calculation differs by as much as a factor of 3 from the impulse approximation, and the impulse approximation calculation for iT_{11} predicts only minute values in contrast to the measured values. The S factor from the full calculation is shown in Fig. 9, and is in good agreement with the experimental data. It is significant to note that the resulting $S(0)$ value is $\sim$25% lower than that found by Griffiths, Lal, and Scarfe [13]. This value is also $\sim$25% lower than the one presently reccomended for use in astrophysical calculations [38].

The PHH calculation only included scattering states with orbital angular momenta $l=0$ and $l=1$. It is possible that the remaining discrepancies, particularly evident for T_{22}, can be removed by the inclusion of higher partial waves. Calculations of these effects are underway.

VI. THERMONUCLEAR REACTION RATE

Since the astrophysical S factor at very low energies found in this work and the recent work of Schmid *et al.* [11] is significantly smaller than that previously assumed, we have reevaluated the thermonuclear reaction rate for this re-

action. The thermonuclear reaction rate $N_A\langle\sigma v\rangle$ is calculated [5] from the cross section σ using

$$N_A\langle\sigma v\rangle=\left(\frac{8}{\pi\mu}\right)^{1/2}\frac{N_A}{(kT)^{3/2}}\int_0^\infty E\sigma(E)\exp\left(-\frac{E}{kT}\right)dE, \qquad (7)$$

where N_A is Avogadro's number, μ is the reduced mass in the entrance channel, k is Boltzmann's constant, T is temperature, and E is the center-of-mass energy. The cross section was taken from the following parametrization of the S factor:

$$S(E)=\begin{cases}0.191+5.09\times10^{-3}E, & \mathrm{E}<100\ \mathrm{keV},\\ 0.700+7.46\times10^{-3}(E-100)+2.96\times10^{-6}(E-100)^2, & E\geqslant100\ \mathrm{keV},\end{cases} \qquad (8)$$

where the units of E and $S(E)$ are keV and eV b, respectively. For $E\leqslant100$ keV, the expression was taken from the calculations of Viviani, Schiavilla, and Kievsky [1], and at higher energies was fitted to experimental data, with the constraint that $S(E)$ is continuous at $E=100$ keV. This expression accurately reproduces the $S(E)$ data found in this work; that of Schmid *et al.* [11] at lower energies; and that of Griffiths, Larson, and Robertson [12] and Bailey *et al.* [14] at higher energies (up to $E\approx1200$ keV). Since the calculations of Viviani, Schiavilla, and Kievsky [1] include a very complete treatment of the relevant physics (see Sec. V), it should provide a more accurate extrapolation to lower energies than a simple linear fit to the S-factor data.

Using this parametrization, the reaction rate was then calculated by numerically integrating Eq. (7). The numerically integrated reaction rate is given within 3% for $T_9\leqslant10$ by the following expression:

$$N_A\langle\sigma v\rangle=1.71\times10^3T_9^{-2/3}\exp\left(-\frac{3.720}{T_9^{1/3}}\right)(1+0.112T_9^{1/3}+2.99T_9^{2/3}+3.89T_9^{4/3}), \qquad (9)$$

where T_9 is the temperature in GK. A comparison of this reaction rate to that used by Smith, Kawano, and Malaney [4], and Caughlin and Fowler [38] is shown in Fig. 10. The new reaction rate is seen to be $\sim30\%$ lower than the previous evaluations for $T_9\lesssim1$, while for $T_9\gtrsim1$ the new rate is significantly higher.

Several tests were carried out to determine the effect of the $^2H(p,\gamma)^3He$ reaction rate on the primordial nucleosynthesis of the light elements ^2H, ^3He, ^4He, and ^7Li. Standard big-bang nucleosynthesis calculations were carried out using the computer code described in Ref. [39]. The calculation assumes that the baryon density is isotropic, and that there are three neutrino species. We find that the final abundance of the light elements depends on the reaction rate in the temperature range $0.2\leqslant T_9\leqslant0.7$; changes in the reaction rate outside of this temperature range do not affect the final abundances (at least for baryon-to-photon ratios in the range $1\leqslant10^{10}\eta\leqslant10$, i.e., where it is believed to lie). This temperature range corresponds approximately to the center-of-mass energy range $15\leqslant E\leqslant400$ keV in the p-d system. We also find that the calculated abundances $^2H/H$, $^3He/H$, $^4He/H$, and $^7Li/H$ are changed less than 10%, compared to calculations using the reaction rate of Smith, Kawano, and Malaney [4]. This change in the reaction rate will not significantly affect models of main-sequence stellar evolution, but it may impact the evolution of low-mass protostars. Further calculations are needed to explore the implications of these results in other astrophysical scenarios.

VII. CONCLUSIONS

In summary, we have carried out the new measurements of the analyzing powers and cross section for low-energy proton-deuteron capture. The theoretical analysis of the data was conducted with an exact three-body model using realistic NN potentials. The data qualitatively agree with the model predictions. The angular distributions of the analyzing powers, especially the vector analyzing powers, confirm that $M1$ transitions play an important role in low-energy p-d capture. Convincing evidence for the presence of MEC effects is found in the comparison of polarization observables with calculations.

The astrophysical S factor and thermonuclear reaction rate have been evaluated on the basis of the available experimental data and the theoretical calculations of Viviani, Schiavilla, and Kievsky [1] which were used for the extrapolation to lower energies. This astrophysical S factor is 25% lower at zero energy than that determined by Griffiths, Lal, and Scarfe [13]. Our experimental results are in good agreement with the recent experiment of Schmid *et al.* [11] at lower energies.

ACKNOWLEDGMENTS

The authors would like to thank Dr. Ben Crowe, Dr. Kurt Fletcher, Dr. Beata Kozlowska, Bill Geist, Kevin Veal, Steve Hale, and Denise Powell for their assistance in the data collection process. We would also like to thank Dr. Greg Schmid for valuable discussions of the proton-deuteron capture reaction. This work was supported in part by the U.S. Department of Energy, Office of High Energy and Nuclear Physics, under Grant No. DE-FG05-88ER40442.

[1] M. Viviani, R. Schiavilla, and A. Kievsky, Phys. Rev. C **54**, 534 (1996).
[2] A. C. Fonseca and D. R. Lehman, Phys. Rev. C **48**, 48 (1993).
[3] A. C. Phillips, Nucl. Phys. **A184**, 337 (1972).
[4] M. S. Smith, L. H. Kawano, and R. A. Malaney, Astrophys. J. Suppl. Ser. **85**, 219 (1993).
[5] C. E. Rolfs and W. S. Rodney, *Cauldrons in the Cosmos* (University of Chicago Press, Chicago, 1988).
[6] S. W. Stahler, Astrophys. J. **332**, 804 (1988).
[7] D. Tytler, X.-M. Fan, and S. Burles, Nature (London) **381**, 207 (1996).
[8] A. Kievsky, S. Rosati, and M. Viviani, Nucl. Phys. **A551**, 241 (1993).
[9] A. Kievsky, S. Rosati, and M. Viviani, Nucl. Phys. **A577**, 511 (1994).
[10] G. J. Schmid, R. M. Chasteler, C. M. Laymon, H. R. Weller, R. M. Prior, and D. R. Tilley, Phys. Rev. C **52**, R1732 (1995).
[11] G. J. Schmid, M. Viviani, B. J. Rice, R. M. Chasteler, M. A. Godwin, G. C. Kiang, L. L. Kiang, A. Kievsky, C. M. Laymon, R. M. Prior, R. Schiavilla, D. R. Tilley, and H. R. Weller, Phys. Rev. Lett. **76**, 3088 (1996).
[12] G. M. Griffiths, E. A. Larson, and L. P. Robertson, Can. J. Phys. **40**, 402 (1962).
[13] G. M. Griffiths, M. Lal, C. D. Scarfe, Can. J. Phys. **41**, 724 (1963).
[14] G. M. Bailey, G. M. Griffiths, M. A. Olivo, and R. L. Helmer, Can. J. Phys. **48**, 3059 (1970).
[15] L. Ma, Ph.D. thesis, University of North Carolina at Chapel Hill, 1995, available from University Microfilms, Ann Arbor, MI 48106.
[16] T. B. Clegg, H. J. Karwowski, S. K. Lemieux, R. W. Sayer, E. R. Crosson, W. M. Hooke, C. R. Howell, H. W. Lewis, A. W. Lovette, H. J. Pfutzner, K. A. Sweeton, and W. S. Wilburn, Nucl. Instrum. Methods Phys. Res. A **357**, 200 (1995).
[17] T. C. Black, B. E. Hendrix, E. R. Crosson, K. A. Fletcher, H. J. Karwowski, and E. J. Ludwig, Nucl. Instrum. Methods Phys. Res. A **333**, 239 (1993).
[18] P. Schwandt, T. B. Clegg, and W. Haeberli, Nucl. Phys. **A163**, 432 (1971).
[19] D. C. Dodder, G. M. Hale, N. Jarmie, J. H. Jett, P. W. Keaton, Jr., R. A. Nisley, and K. White, Phys. Rev. C **15**, 518 (1977).
[20] S. A. Tonsfeldt, Ph.D. thesis, University of North Carolina at Chapel Hill, 1981, available from University Microfilms, Ann Arbor, MI 48106.
[21] W. H. Geist, Z. Ayer, A. C. Hird, H. J. Karwowski, and E. J. Ludwig, Nucl. Instrum. Methods Phys. Res. A **365**, 36 (1995).
[22] K. I. Hahn, C. R. Brune, and R. W. Kavanagh, Phys. Rev. C **51**, 1624 (1995).
[23] R. Brun, CERN Program Library Q121, CERN (1993).
[24] H. H. Jorsch and J. L. Campbell, Nucl. Instrum. Methods **143**, 551 (1977).
[25] J. F. Ziegler, TRIM92 User Manual, IBM-Research, 1992.
[26] W. A. Wenzel and W. Whaling, Phys. Rev. **87**, 499 (1952).
[27] F. James, Comput. Phys. Commun. **20**, 29 (1980).
[28] R. G. Seyler and H. R. Weller, Phys. Rev. C **20**, 453 (1979).
[29] F. Goeckner, W. K. Pitts, and L. D. Knutson, Phys. Rev. C **45**, R2536 (1992).
[30] S. King, N. R. Roberson, H. R. Weller, D. R. Tilley, H. P. Engelbert, H. Berg, E. Huttel, and G. Clausnitzer, Phys. Rev. C **30**, 1335 (1984).
[31] A. Kievsky, M. Viviani, and S. Rosati, Phys. Rev. C **52**, R15 (1995).
[32] R. B. Wiringa, V. G. J. Stoks, and R. Schiavilla, Phys. Rev. C **51**, 38 (1995).
[33] B. S. Pudliner, V. R. Pandharipande, J. Carlson, and R. B. Wiringa, Phys. Rev. Lett. **74**, 4396 (1995).
[34] R. Schiavilla, R. B. Wiringa, V. R. Pandharipande, and J. Carlson, Phys. Rev. C **45**, 2628 (1992).
[35] R. Schiavilla and D. O. Riska, Phys. Rev. C **43**, 437 (1991).
[36] R. B. Wiringa, Phys. Rev. C **43**, 1585 (1991).
[37] D. O. Riska, Phys. Scr. **31**, 471 (1985).
[38] G. R. Caughlin and W. A. Fowler, At. Data Nucl. Data Tables **40**, 283 (1988).
[39] L. H. Kawano, NUC123 computer code (1992); Caltech Kellogg Radiation Lab Report OAP-714; Fermilab Report No. FERMILAB-PUB-92/04-A.